Concise Report

Vibrational signal detection, Flexible broad-range, Sensors, Conducting materials, Polymers

CJC Chinese Journal of Chemistry 中国化学 An International Journal

Flexible Broad-Range Pressure Sensors Enabled by Deformation-Induced Conductive Channels in 3D Graphene Foam@Polydimethylsiloxane Composite for Precise Vibrational Signal Detection

Jiankun Miao,[a,b] Yayuan Shi,[b] Hongfei Zhu,*[,b] and Mingyi Gao*[,a]

[a] *Suzhou Key Laboratory of Advanced Optical Communication Network Technology, School of Electronic and Information Engineering, Soochow University, Suzhou, Jiangsu 215006, China*
[b] *Department of Chemistry, Rowey Intelligent Technology (Suzhou) Ltd., Co., High-tech Zone, Suzhou, Jiangsu 215011, China*

Cite this paper: *Chin. J. Chem.* **2020**, *38*, 719—724. **DOI: 10.1002/cjoc.201900538**

Summary of main observation and conclusion Here we report the design and fabrication of high-performance pressure sensors based on three-dimensional (3D) graphene foam filled polydimethylsiloxane (GF@PDMS) composite with a broad sensing range spaning from 0.05 kPa to 130 kPa. The interpretation of device functioning mechanism can be classified into low and high pressure sensing regions. In the low pressure region (<15 kPa), the pressure loading leads to the temporal connection of micro-cracks in GF scaffold and forming conductive channels. In the high pressure region (15 kPa to 130 kPa), the pressure induced deformation of GF results in the better connections among micro-cracks and the shortening of conductive pathway to further decrease the electrical resistance. The GF@PDMS sensors exhibited accuracy, sensibility and reproducibility to detect pressure signals with remarkable stability for over 16000 loading-unloading cycles, indicating its great potential for practical applications. Moreover, the GF@PDMS sensors also showed high performances in the detection of dynamic pressures, such as subtle mechanical vibration signals, as well as physiology vibrational signals generated by human throats. We expect this technology could be integrated into different sensing systems for the applications in wearable smart electronics and human-machine communications.

Background and Originality Content

Flexible, sensitive, and cost-efficient pressure sensors with broad sensing range are highly desirable for the fabrication of next-generation portable devices. Most researches on pressure sensors are based on expensive thin film deposition, micro-fabrication and lithography techniques.[1-3] However, the large-scale fabrication of pressure sensors with these semiconductor techniques is expensive and complicated, especially in the case of broad-range deformation detection. To conquer these limitations, several high efficiency and scalability methods are developed, such as, laser micro-engineering,[4-6] UV interface processing,[7] template-duplication,[8] 3D printing.[9] Besides these newly developed techniques, flexible and malleable pressure sensors with non-fragile materials also hold great promise to overcome these problems.[10,11] For instance, two-dimensional (2D) graphene sheets with remarkable electrical and mechanical properties[12] were integrated into macroscopic structures for the fabrication of novel pressure sensors.[13-15] However, there are still some remaining challenges to design high-performance flexible pressure sensors based on conductive nanocarbon fillers and elastic polymer matrix.[14,16-18] Especially, the pressure sensing range, the device durability during loading-unloading cycles, and the dynamic pressure (vibration) sensibility of state-of-the-art flexible pressure sensors are still not fully satisfying. Furthermore, many research works are focused on the fabrication of pressure sensors, while the functioning mechanism and relationship between the composite structure and sensing performance are still not well understood.

Herein, we report a procedure for the construction of high-performance pressure sensors based on three-dimensional (3D) graphene foam filled polydimethylsiloxane (GF@PDMS) composite. The GF@PDMS sensors can detect broad-range pressures, such as low-pressure physiology vibrational signals and high-pressure mechanical deformation zones.[13,19] The pressure sensing properties in *z*-direction and the functional mechanism of these pressure sensors were systematically investigated. The excellent sensing capability of the GF@PDMS sensor at low pressure is attributed to the formation and disconnection of the conductive channels between the micro-cracks in GF@PDMS composite during loading-unloading cycles. Moreover, the good elasticity of PDMS matrix provides remarkable reproducibility for the detection of high pressure, and also contributes to the great device durability with almost no performance degradation upon 16000 loading-unloading cycles of aging test. The GF@PDMS pressure sensors have the advantages of high accuracy, fast response, excellent stability and cost efficiency. Furthermore, the GF@PDMS sensors can be used to precisely detect dynamic pressure (vibration), such as the vibrational signals of motors and the physiological vibration signals of human throats.

Results and Discussion

The fabrication process of GF@PDMS based pressure sensors is shown in Figure 1a. Firstly, few-layer graphene was grown on pre-cleaned Ni foam by chemical vapor deposition (CVD) method (Figures 1b and 1c).[7,13] The GF covered Ni foam (Ni@GF) was etched in a mixed aqueous solution of $Fe(NO_3)_2$ and HCl for 3 h and washed by deionized water to obtain free-standing GF (Figure 1d). The GF was sandwiched between two Japanese Toray carbon paper (CP) electrodes, and viscous PDMS monomer was filled into GF framework and then solidified at 90 °C for 20 min to obtain GF@PDMS based pressure sensor. Figure 1e shows the scanning electron microscopy (SEM) image of the cross-section of GF@PDMS composite, revealing the integration of conductive GF framework and elastic PDMS matrix. Figures 1f and 1g present the device structure of GD@PDMS pressure sensor connected with two flexible and conductive CP electrodes. Raman spectroscopy

*E-mail: zhuhf@iccas.ac.cn, mygao@suda.edu.cn

For submission: https://mc.manuscriptcentral.com/cjoc
For articles: https://onlinelibrary.wiley.com/journal/16147065

characterizations were performed on the samples of pristine Ni foam, pristine PDMS, Ni@GF and freestanding GF. The Raman spectrum of Ni@GF (brown curve in Figure 1h) shows no D band, indicating the high quality of GF framework. However, a small D band appears in the Raman spectrum of free-standing GF after the etching of Ni foam, probably owing to the formation of trace defects during the etching process.

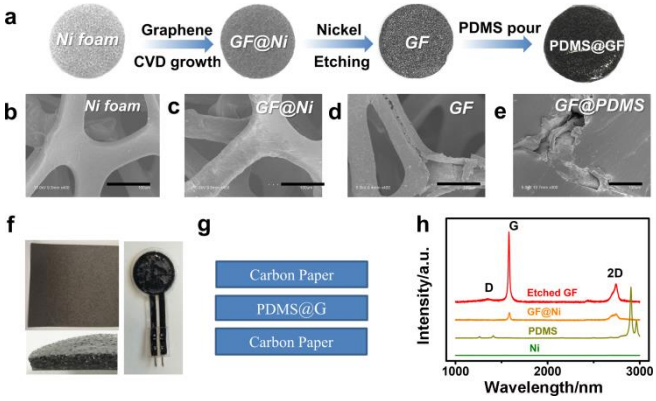

Figure 1 The fabrication of GF@PDMS based pressure sensors. (a) Schematic fabrication process of GF@PDMS pressure sensors. (b—e) SEM images of (b) pristine Ni foam, (c) Ni@GF, (d) free-standing GF after the etching of Ni foam, and (e) the cross-section of as-prepared GF@PDMS composite. Scale bars: 100 μm. (f) Photographs of a flexible carbon paper electrode (left top), cross-section of GF@PDMS material (left bottom) and the as prepared GF@PDMS pressure sensor (Right). (g) Schematic 3D stereostructure of GF@PDMS pressure sensor. (h) Raman spectra of pristine Ni foam, pristine PDMS, Ni@GF and freestanding GF after the etching of Ni foam.

To study the pressure detection properties, the GF@PDMS sensor was mechanically pressed by a step motor equipped with a force gauge (Figure 2a) and controlled by a computer-programmed motor controller. The schematic illustration of this set-up is shown in Figure 2b. In this work, all the device electrical properties were monitored with an electrical source meter at a fixed applied voltage 0.1 V. To make the pressure sensor suitable for practical applications, it is necessary to ensure good material durability and high device stability. Therefore, a device aging process of 16000 loading-unloading cycles was performed at a pressure of 30 kPa (Figure 2c). Some typical loading-unloading cycles were magnified and shown in the inset of Figure 2c. It was found that the sensor exhibited excellent durability toward aging, which could be attributed to the good flexibility and stability of PDMS. There are two purposes for this aging process: (i) to introduce more micro-cracks in the carbon scaffold of GF to achieve better sensibility for detecting low dynamic pressure signals, such as mechanical vibration and acoustic vibration;[8] (ii) to ensure the long-term durability and signal repeatability of the conductive network in the GF@PDMS composite.

To characterize the compressing and recovery behaviors of the sensor, the device current was monitored at different step motor moving distances from 0, 25, 50, 75 to 100 μm (each step was held for 10 s) with the corresponding applied pressure increased from 0, 0.9, 3.0, 7.9 to 19 kPa, respectively (Figure 2c). Then, the compression was gradually recovered from 100 to 0 μm, with the corresponding pressure decreased from 19, 7.7, 2.8, 0.8 to 0 kPa, as illustrated in Figure 2c. The relationship between the step motor moving distance and the applied pressure is depicted in Figure 2d, indicating the good reversibility of GF@PDMS based sensor.

The response time is one of the most important parameters for pressure sensors, which can be defined as the time required for the output signal increasing from 10% to 90% of the peak output value, or vice versa.[14,15,20,21] The GF@PDMS based sensor showed a relatively fast response time towards the variation of pressure. Considering the repeatable experimental results, one typical loading-unloading cycle in Figure 2b was picked out for interpreting the relationship between the applied pressure and device current response. Upon loading, the device current will increase rapidly to 90% of the peak current value in 0.8 s (Figure 2e). After holding the pressure for 10 s and then releasing, the current will drop rapidly (in 0.2 s) towards a low current level.

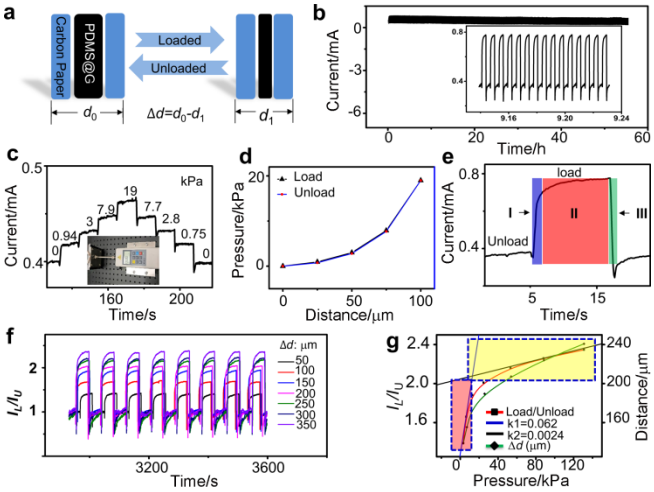

Figure 2 Force sensing properties of GF@PDMS based pressure sensor. (a) Schematic illustration of GF@PDMS based pressure sensor in loading and unloading states. d_0 represents the original thickness of the GF@PDMS sensor in unloading state, d_1 stands for the sensor thickness in loading states, Δd is the sensor thickness deformation value between unloading and loading states. (b) Aging experiments of GF@PDMS based pressure sensor at an applied pressure of 30 kPa for 16000 cycles. The inset shows typical loading-unloading cycles of the sensor. (c) Device current as the function of stepwise changed loading force on the sensor. The inset shows apparatus setup. (d) Pressure applied on the sensor as the function of device deformation in loading and unloading states. (e) Device response times during the loading (0.8 s) and unloading (0.2 s) processes. (f) Specific value of device current in load and unload states (I_L/I_U) at different thickness deformation value (from 50—350 μm) of the sensor compressed by force gauge. I_L represents the real-time device current in loading state, and I_U is the device current in unloading state. (g) The relationships of loading pressure vs. I_L/I_U ratio (experimental results: black square dots; fitted data: red curve) and loading pressure vs. step motor moving distance (blue triangle line). The red and yellow regions represent low and high pressure sensing zones, respectively.

The interaction process of GF@PDMS based pressure sensor can be divided into three working stages in a single loading-unloading cycle: (i) Low pressure interacting stage (blue area in Figure 2e). This stage would span from the initial contact between the force gauge and the pressure sensor until the device current increased to 90% of the peak output value. We suggest that the pressure sensitivity of GF@PDMS based sensor at low pressure region (<15 kPa) is determined by the conductivity variation of GF scaffold with temporally-connected micro-cracks under compressive stress, which is similar to a previous report.[8] (ii) High pressure interacting stage (red area in Figure 2e). This stage spans from 90% to 100% of the peak current value. The relatively long saturate time could be ascribed to the gradual formation of more conductive channels in GF scaffold and the shortening of conductive pathway under pressing.[16,22] (iii) Pressure releasing stage (green area in Figure 2e). When the pressure is released, the current will drop rapidly in 0.2 s from 90% to 10% of the peak output

value. This is understandable if considering the working frequency (50 Hz) of step motor, which is adequate to move to the unloading position without affecting the device response time. In this process, the rapid drop of device current is due to the recovery of micro-cracks and the disconnection of temporal conductive channels after the release of elastic PDMS matrix from compressing stress.

To verify the assumption that there are low-pressure and high-pressure sensitive zones in this sensor, a series of device thickness deformation values from 50—350 μm, which results in a series of pressure from low (3 kPa) to high (130 kPa), were employed to study the developing trend of sensor performance.[17,23] Detailed data was shown in Table 1. To study how the pressure influences the device performance, the peak values of I_L/I_U as the function of different loading pressures were depicted in Figure 2g (black square dots). With the increase of loading pressure, the peak value of I_L/I_U will also increase, but not always grow linearly. The fitted data (red curve in Figure 2g) of the experimental results can be expressed as an ambi exponent Equation (1):

$$y = -0.93\exp\left(-\frac{x}{4.9}\right) - 0.64\exp\left(-\frac{x}{98.01}\right) + 2.52 \quad (1)$$

where y represents the peak value of I_L/I_U, and x represents the loading pressure. Moreover, the step motor moving distance also exhibits a similar variation tendency related to the loading pressure, as indicated by the blue triangle line in Figure 2g. The physical meaning of this ambi exponential growth phenomenon indicates two kinds of sensing modes of the sensor: the low-pressure sensing mode (red shaded part in Figure 2g) and the high-pressure sensing mode (yellow shaded part in Figure 2g). It was found that the peak value of I_L/I_U increased rapidly when pressure increased from 0 to 15 kPa (low pressure zone). This could be ascribed to the formation of many temporal interlinks among the micro-cracks in GF scaffold under low pressure to generate abundant conductive channels.[8,14,17,23] In this sensing region, device sensitivity is around 0.062 kPa^{-1} (blue line in Figure 2g). While in the high-pressure zone (15 to 130 kPa), the peak value of I_L/I_U gradually increased along the loading pressure and approached a saturation value of about 2.52, as shown in Equation (2):

$$\lim_{x\to+\infty} y = \lim_{x\to+\infty}\left(-0.93\exp\left(-\frac{x}{4.9}\right) - 0.64\exp\left(-\frac{x}{98.01}\right) + 2.52\right) = 2.52 \quad (2)$$

The gradual increase of the peak value of I_L/I_U in high pressure zone should be attributed to the formation of better connections among micro-cracks at high pressure and the shortening of current transport distance under compression, which both further decreased the device resistance. This analysis is in correspondence with the above-mentioned assumption for interpreting the three working stages in a single loading-unloading cycle. In this sensing region, device sensitivity is around 0.0024 kPa^{-1} (black line in Figure 2g).

Table 2 demonstrates the characteristics comparison of recently reported pressure sensors and GF@PDMS based broad range sensor. It was found that the sensor in this work exhibits the broad range sensibility and high stability.

Table 1 The functioning parameters of GF@PDMS pressure sensor pressed by force gauge.

	Δd/μm	Pressure/kPa	Force/N	On/Off ratio
1	50	3	1.6	1.4
2	100	6.75	3.6	1.67
3	150	11.32	6.0	1.9
4	200	25.45	13.5	2
5	250	53.29	28.3	2.16
6	300	88.37	46.9	2.26
7	350	130.3	69.2	2.35

Note: The "Δd" represents the thickness deformation value of the sensor, "force" and "pressure" stand for the device sensed force and pressure imposed by force gauge. On/Off ratio is the specific value of device current in load and unload states. The radius of the sensor is around 13 mm.

Table 2 The comparison of characteristics pressure sensors of recently reported

	DR/kPa	S/kPa^{-1}	DL/kPa	RT/s	LTS/cycle	Ref.
1	0—10	–1.82	0.001	0.036	6000	[4]
2	0—1.4	–5.5	0.0015	0.0002	5000	[24]
3	0.007—50	–1.01	0.007	0.01	5000	[7]
4	0.2—59	15.1	0.0002	0.04	—	[8]
5	—	–0.111	0.02	0.1 s	10000	[25]
5	0—9	–2.5	0.015	0.02	—	[5]
6	0.05—130	0.062	0.01	0.2 s	16000	TW

Note: DR: detection range; S: sensitivity; MDL: detection limit; RT: Response time; LTS: long-term stability; TW: this work.

The sensitivity of GF@PDMS based pressure sensor at low pressure is mainly attributed to the pressure-induced formation of conductive channels through the connection of micro-cracks in the GF scaffold, as illustrated in Figure 3a. The presence of micro-cracks in the pristine GF scaffold and the cross-section of GF@PDMS composite is confirmed by SEM characterizations (Figures 3b and 3c). As we proposed above, the micro-cracks can temporarily connect together under low pressure to form more conductive channels, greatly increasing the device conductivity. When the pressure is released, the high elasticity of PDMS matrix will make these conductive channels disconnected again. At high pressure zone, the amount of conductive channels will be further increased by compression (but with lower growth rate), and gradually approach a saturated level.

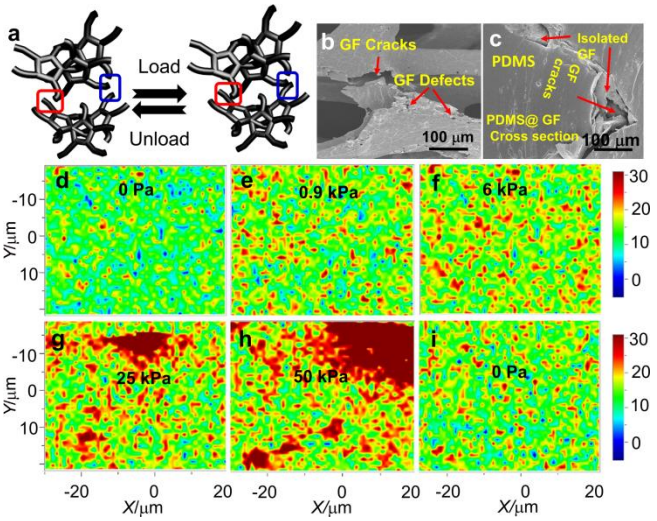

Figure 3 Functioning mechanism and in-situ Raman characterizations of GF@PDMS based pressure sensor. (a) Schematic illustration of the connection and disconnection of micro-cracks in GF scaffold upon loading and unloading cycles. (b) SEM image of a micro-crack in GF scaffold. (c) SEM image of the cross-section of GF@PDMS composite with micro-cracks in GF scaffold. (d—i) In-situ Raman mappings of the cross-section of GF@PDMS composite under the pressure of (d) 0 kPa, (e) 0.9 kPa, (f) 6 kPa, (g) 25 kPa, (h) 50 kPa and (i) 0 kPa, respectively.

To study the microstructure variation of the elastic GF@PDMS composite under loading pressure, in-situ Raman spectroscopy characterizations were carried out through the mapping of peak

intensities at a fixed Raman shift of 1580 cm^{-1}, corresponding to the G band of graphene.[18,19,26,27] The Raman signals were collected at the same area of GF@PDMS composite compressed by a glass slide under different loading pressures (Figures 3d—3i). In the unloading state, the measured Raman signals of G band were weak throughout the mapping area, indicating that the PDMS matrix coated on GF scaffold covered up the Raman signals (Figure 3d). At low pressures (0.9 kPa and 6 kPa), stronger G band signals would appear within the mapping area, but still not very apparent (Figures 3e, 3f). This might be because the low pressure (<15 kPa) merely influences the connection of micro-cracks in the composite, but doesn't change the morphology of the composite material much. When the loading pressure was increased to 25 kPa, much stronger G band signals appeared at different sites in the mapping area (Figure 3g). By further increasing the loading pressure to 50 kPa, the strong G band signals will be expanded to larger areas (Figure 3h). This indicates that the high compression ratio under high pressure would shorten the distance between the PDMS-concealed GF scaffold and the composite surface, thus the G band signals can be emerged over a large area. This suggests that the shortening of current pathway plays a key role on the gradually increased device conductivity induced by the stronger stress at high pressure region (Figure 2i). After unloading the pressure, the G peak intensity of Raman mapping will restore to a low level comparable to the original state (Figure 3i). This is because the high elasticity of PDMS matrix can help the composite return to its original morphology.

The combination of crack-rich GF scaffold and elastic PDMS matrix offers the possibility for precisely sensing the loading pressure. In GF@PDMS composite, each component has their own roles. For the 3D-interconnected GF scaffold, it provides an integrated conductive framework for rapid charge transfer, which is the reason for the high conductivity of GF@PDMS that is several orders of magnitude higher than those of CNT@polymer composite materials.[7,13,20,28] Moreover, the temporal connection and disconnection of micro-cracks in GF scaffold facilitates the drastic and rapid variation of conductive channels under different pressures. For the PDMS matrix, it serves as a support skeleton for the protection of GF and retaining conductive channels from high stress. Moreover, the PDMS matrix offers high elasticity for the rapid and full recovery from pressing. This is especially important for the sensor to resist the high pressure.

Besides static pressure, the GF@PDMS based pressure sensor can also precisely detect subtle dynamic vibrational and acoustical signals. Vibration is periodic or random mechanical oscillation occurring around an equilibrium point. The vibration signals of industrial machinery are vital indicators of the machinery health. For the sensing of vibration, high-performance sensors with fast response, high accuracy and excellent reproducibility are required.[29] To explore the potential of practical applications in industry and in daily life,[30,31] we demonstrate that the GF@PDMS sensor can be used to detect the different vibration modes of cell phone. The sensor was placed on a cell phone (Figure 4a) to detect the long-term stability in dynamic low-pressure zone (Figure 4b). It was found that the device exhibits high stability as in high-pressure zone. To further characterize device reproductivity, the cell phone was set at vibration mode, and three different vibration modes (Heartbeat, S.O.S., and Symphony) were chosen for demonstration, as shown in Figures 4c—4e. It was found that the change of vibration modes would generate different device current profiles of the sensor (Figures 4c—4e), and the repeating cycles of these vibration modes can be clearly identified. The high reproducibility of the periodic vibrations detected by the sensor indicated its good sensitivity and consistency, which are the primary consideration factors for commercial applications.

Considering the sensitivity of GF@PDMS sensor in low pressure zone, it is also promising to use it for monitoring physiological vibration signals. As a typical physiological signal, the acoustical signals produced by human throats are critically important for human-computer communication and speech recognition. It is highly desirable to develop low-cost and high-performance portable sensors for the real-time detection of personal acoustical signals. We demonstrate that the GF@PDMS sensor attached on human throat can be applied for detecting individual pronunciation through throat vibration (as inset in Figure 5a). For example, the English pronunciation of different numbers (from "one" to "ten") produced distinguishable current profiles (Figure 5a). The throat vibrational signals of three repeatedly pronounced numbers ("one", "three" and "five") were recorded (Figures 5b—5d), showing similar current profiles within repeated cycles. This indicates the high reproducibility of GF@PDMS sensor for the detection of individual physiology vibrational signals. To further prove

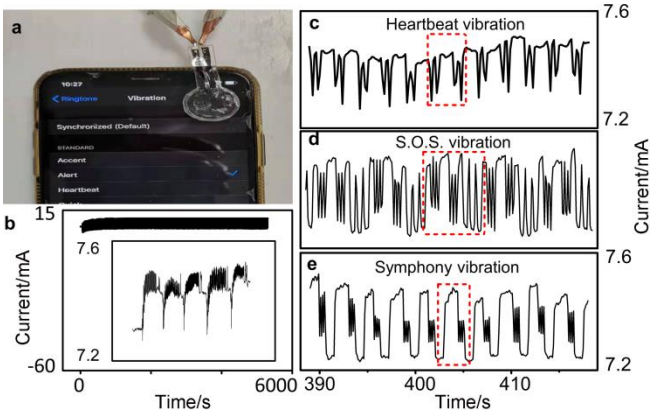

Figure 4 Vibrational signal detection enabled by GF@PDMS based pressure sensor. (a) Optical image of the setup for the detection of subtle vibration generated by an iPhone X. (b) Aging experiments of GF@PDMS based pressure sensor at dynamic pressure (around 10 Pa) for around 5000 seconds. The inset shows typical iPhone X vibrational signals detected by the sensor. (c—e) Repeated vibrational signals provided by the cell phone: (c) Heartbeat, (d) S.O.S. and (e) Symphony vibration modes detected by GF@PDMS sensor.

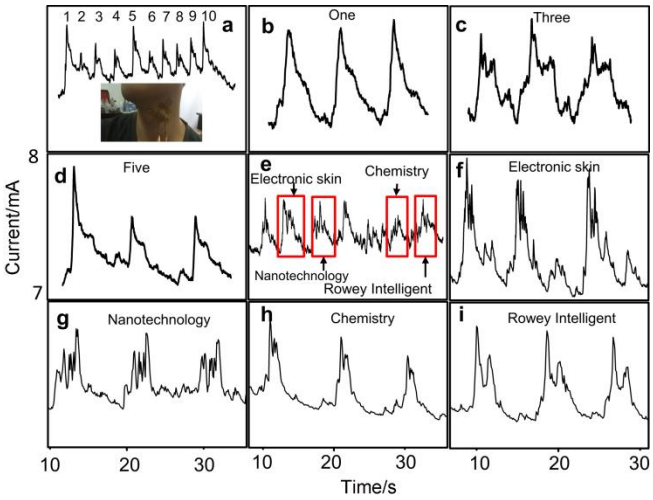

Figure 5 Physiology vibrational signal detected by the GF@PDMS sensor. (a) vibrational signals of English pronunciation of different numbers (from "one" to "ten"). The inset shows optical images of the setup for the detection of physiology vibrational signals generated by human throat. (b—d) Typical three-repeated throat vibrational signals of English pronunciation of (b) "one", (c) "three" and (d) "five". (e) The vibrational signals of a sentence: "The electronic skin nanotechnology was developed in the Department of Chemistry in Rowey Intelligent." (f—i) Typical three-repeated throat vibrational signals of English pronunciation of (f) electronic skin; (g) nanotechnology; (h) Chemistry; (i) Rowey Intelligent.

the excellent reproducibility of GF@PDMS sensor, the vibrational signals of a sentence was detected: "The electronic skin nanotechnology was developed in the Department of Chemistry in Rowey Intelligent." When pick out and speak three times of the four phrases: electronic skin (Figure 5f), nanotechnology (Figure 5g), Chemistry (Figure 5h), Rowey Intelligent (Figure 5i), it was found that the vibrational signals of these phrases are highly coincident with the phrases signals in the sentence above. Vibrational signal detection can be applied in the communication between doctors and patients who is in the case of loss of voice.

Conclusions

In summary, the GF@PDMS based sensor exhibited broad-range pressure sensing capability, good reproducibility and long-term stability. The pressure sensitivity of the sensor at low pressure region (<15 kPa) should be attributed to the conductivity variation of GF scaffold with temporally-connected micro-cracks under pressure. At high pressure region (15 to 130 kPa), the sensing mechanism could be ascribed to the formation of better connection between micro-cracks in GF scaffold and the shortening of conductive pathway by compression. Furthermore, the GF@PDMS sensor also exhibited high performance for the detection of subtle mechanical vibration and physiological acoustical signals. Considering the easy preparation process and low cost, we suggest the GF@PDMS sensor is promising for practical applications in the future, such as human-machine communications and wearable electronics.

Experimental

Fabrication of GF@PDMS sensor. Ni foams (0.8 g·cm^{-3} in density and 0.7 mm in thickness, purchased from Taili New Energy Corp., Suzhou) were used as 3D scaffold templates for the growth of GFs by CVD method.[7] Briefly, Ni foam was firstly heated in a horizontal quartz tube furnace at 1000 °C for 5 min with the gas flow of 100 sccm Ar and 200 sccm H_2 to clear the thin surface oxide layer. Then, 15 sccm of CH_4 flow was introduced into the quartz tube together with the Ar/H_2 mixture flow and reacted for 5 min. The furnace was rapidly cooled to room temperature under Ar flow (100 sccm) to obtain Ni@GF. To prevent structural failure of GF, the Ni@GF was mildly etched with 500 mL of saturated $Fe(NO_3)_3$ solution mixed with 2 mL of 37% HCl at 80 °C for 3 h. The free-standing GF was washed 4 times with deionized water and dried naturally overnight. To fabricate GF@PDMS sensor, two CP electrodes were placed at the bottom and top surfaces of the free-standing GF, respectively, and then the base/curing agent mixture of PDMS (Sylgard 184, Dow Corning) was cast onto it. After curing at 90 °C for 20 min, the flexible GF@PMDS pressure sensor was obtained.

Characterizations. Scanning electron microscopy (SEM) images of the samples were collected on a FEI Nova-450 instrument. Raman mapping analysis was carried out with a Horiba JY LabRam HR Evolution Raman spectrometer.

Device measurements. The GF@PDMS pressure sensor was mechanically pressed with a motor-controlled stepper (purchased from Beijing Optical Century Instrument Corp.). The electrical properties of pressure sensor were measured with a fixed applied voltage 0.1 V. The current-voltage and current-time curves of the as-prepared devices were collected with a Keithley 2635 source meter.

Acknowledgement

This work was supported by the Project of 2018 Leading Talents of Science and Technology Innovation and Entrepreneurship in Suzhou High Tech Zone ((2018)113#), Project of 2019 Gusu Leading Talents of Science and Technology Innovation and Entrepreneurship (ZXL2019229), Suzhou Industry Technological Innovation Projects (SYG201809), and National Natural Science Foundation of China (NSFC) (61307082).

References

[1] Wang, Y.; Chodavarapu, V. P. Wide-temperature range CMOS capacitance to digital convertor for MEMS pressure sensors. *Sens. Actuators A-Phys.* **2015**, *233*, 302–309.

[2] Choong, C.-L.; Shim, M.-B.; Lee, B.-S.; Jeon, S.; Ko, D.-S.; Kang, T.-H.; Bae, J.; Lee, S. H.; Byun, K.-E.; Im, J.; Jeong, Y. J.; Park, C. E.; Park, J.-J.; Chung, U. I. Highly Stretchable Resistive Pressure Sensors Using a Conductive Elastomeric Composite on a Micropyramid Array. *Adv. Mater.* **2014**, *26*, 3451–3458.

[3] Gutruf, P.; Zeller, E.; Walia, S.; Nili, H.; Sriram, S.; Bhaskaran, M. Stretchable and Tunable Microtectonic ZnO-Based Sensors and Photonics. *Small* **2015**, *11*, 4532–4539.

[4] Yang, G.; Cong, L.; Yu, G.; Jin, S.; Tan, J.; Xuan, F. Laser micro-structured pressure sensor with modulated sensitivity for electronic skins. *Nanotechnology* **2019**, *30*, 325502.

[5] Andreia dos Santos, A.; Pinela, N.; Alves, P.; Santos, R.; Fortunato, E.; Martins, R.; Águas, H.; Igreja, R. Piezoresistive E-Skin Sensors Produced with Laser Engraved Molds. *Adv. Electron. Mater.* **2018**, *4*, 1800182.

[6] Lu, C.; Gao, Y.; Yu, G.; Xu, M.; Tan, J.; Xuan, F. Laser-microengineered flexible electrodes with enhanced sensitivity for wearable pressure sensors. *Sens. Actuators A-Phys.* **2018**, *281*, 124–129.

[7] Yu, G.; Hu, J.; Tan, J.; Gao, Y.; Lu, Y.; Xuan, F. A wearable pressure sensor based on ultra-violet/ozone microstructured carbon nanotube/polydimethylsiloxane arrays for electronic skins. *Nanotechnology* **2018**, *29*, 115502.

[8] Park, J.; Lee, Y.; Hong, J.; Ha, M.; Jung, Y.-D.; Lim, H.; Kim, S. Y.; Ko, H. Giant Tunneling Piezoresistance of Composite Elastomers with Interlocked Microdome Arrays for Ultrasensitive and Multimodal Electronic Skins. *ACS Nano* **2014**, *8*, 4689–4697.

[9] Gao, Y.; Yu, G.; Shu, T.; Chen, Y.; Yang, W.; Liu, Y.; Long, J.; Xiong, W.; Xuan, F. 3D-Printed Coaxial Fibers for Integrated Wearable Sensor Skin. *Adv. Mater. Technol.* **2019**, *4*, 1900504.

[10] Segev-Bar, M.; Landman, A.; Nir-Shapira, M.; Shuster, G.; Haick, H. Tunable Touch Sensor and Combined Sensing Platform: Toward Nanoparticle-based Electronic Skin. *ACS Appl. Mater. Inter.* **2013**, *5*, 5531–5541.

[11] Park, M.; Park, Y. J.; Chen, X.; Park, Y.-K.; Kim, M.-S.; Ahn, J.-H. MoS_2-Based Tactile Sensor for Electronic Skin Applications. *Adv. Mater.* **2016**, *28*, 2556–2562.

[12] Novoselov, K. S.; Geim, A. K.; Morozov, S. V.; Jiang, D.; Zhang, Y.; Dubonos, S. V.; Grigorieva, I. V.; Firsov, A. A. Electric field effect in atomically thin carbon films. *Science* **2004**, *306*, 666–669.

[13] Chen, Z.; Ren, W.; Gao, L.; Liu, B.; Pei, S.; Cheng, H.-M. Three-dimensional flexible and conductive interconnected graphene networks grown by chemical vapour deposition. *Nat. Mater.* **2011**, *10*, 424–428.

[14] Yao, H.-B.; Ge, J.; Wang, C.-F.; Wang, X.; Hu, W.; Zheng, Z.-J.; Ni, Y.; Yu, S.-H. A Flexible and Highly Pressure-Sensitive Graphene-Polyurethane Sponge Based on Fractured Microstructure Design. *Adv. Mater.* **2013**, *25*, 6692–6698.

[15] Tian, H.; Shu, Y.; Wang, X.-F.; Mohammad, M. A.; Bie, Z.; Xie, Q.-Y.; Li, C.; Mi, W.-T.; Yang, Y.; Ren, T.-L. A Graphene-Based Resistive Pressure Sensor with Record-High Sensitivity in a Wide Pressure Range. *Sci. Rep.* **2015**, *5*, 8603.

[16] Pang, C.; Lee, G.-Y.; Kim, T.-i.; Kim, S. M.; Kim, H. N.; Ahn, S.-H.; Suh, K.-Y. A flexible and highly sensitive strain-gauge sensor using reversible interlocking of nanofibres. *Nat. Mater.* **2012**, *11*, 795–801.

[17] Lipomi, D. J.; Vosgueritchian, M.; Tee, B. C. K.; Hellstrom, S. L.; Lee, J. A.; Fox, C. H.; Bao, Z. Skin-like pressure and strain sensors based on transparent elastic films of carbon nanotubes. *Nat. Nanotechnol.*

2011, *6*, 788–792.
[18] Hammock, M. L.; Chortos, A.; Tee, B. C. K.; Tok, J. B. H.; Bao, Z. 25th Anniversary Article: The Evolution of Electronic Skin (E-Skin): A Brief History, Design Considerations, and Recent Progress. *Adv. Mater.* **2013**, *25*, 5997–6037.
[19] Dagdeviren, C.; Su, Y.; Joe, P.; Yona, R.; Liu, Y.; Kim, Y.-S.; Huang, Y.; Damadoran, A. R.; Xia, J.; Martin, L. W.; Huang, Y.; Rogers, J. A. Conformable amplified lead zirconate titanate sensors with enhanced piezoelectric response for cutaneous pressure monitoring. *Nat. Commun.* **2014**, *5*, 4496.
[20] Lee, J.; Kwon, H.; Seo, J.; Shin, S.; Koo, J. H.; Pang, C.; Son, S.; Kim, J. H.; Jang, Y. H.; Kim, D. E.; Lee, T. Conductive Fiber-Based Ultrasensitive Textile Pressure Sensor for Wearable Electronics. *Adv. Mater.* **2015**, *27*, 2433–2439.
[21] Tang, F.; Chen, Q.; Chen, L.; Ye, F.; Cai, J.; Chen, L. Mixture interlayer for high performance organic-inorganic perovskite photodetectors. *Appl. Phys. Lett.* **2016**, *1*09, 123301.
[22] Pan, L.; Chortos, A.; Yu, G.; Wang, Y.; Isaacson, S.; Allen, R.; Shi, Y.; Dauskardt, R.; Bao, Z. An ultra-sensitive resistive pressure sensor based on hollow-sphere microstructure induced elasticity in conducting polymer film. *Nat. Commun.* **2014**, *5*, 3002.
[23] Zang, Y.; Zhang, F.; Di, C.-a.; Zhu, D. Advances of flexible pressure sensors toward artificial intelligence and health care applications. *Mater. Horiz.* **2015**, *2*, 140–156.
[24] Zhu, B.; Niu, Z.; Wang, H.; Leow, W. R.; Wang, H.; Li, Y.; Zheng, L.; Wei, J.; Huo, F.; Chen, X. Microstructured Graphene Arrays for Highly Sensitive Flexible Tactile Sensors. *Small* **2014**, *10*, 3625–3631.
[25] Xu, M.; Gao, Y.; Yu, G.; Lu, C.; Tan, J.; Xuan, F. Flexible pressure sensor using carbon nanotube-wrapped polydimethylsiloxane microspheres for tactile sensing. *Sens. Actuators A-Phys.* **2018**, *284*, 260–265.
[26] Guo, X.; Bi, H.; Zafar, A.; Liang, Z.; Shi, Z.; Sun, L.; Ni, Z. Investigation of dodecane in three-dimensional porous graphene sponge by Raman mapping. *Nanotechnology* **2016**, *27*, 055702.
[27] Hoffmann, G. G.; Barsan, O. A.; van der Ven, L. G. J.; de With, G. Tip-enhanced Raman mapping of single-walled carbon nanotube networks in conductive composite materials. *J. Raman Spectrosc.* **2017**, *48*, 191–196.
[28] Hu, N.; Karube, Y.; Yan, C.; Masuda, Z.; Fukunaga, H. Tunneling effect in a polymer/carbon nanotube nanocomposite strain sensor. *Acta Mater.* **2008**, *56*, 2929–2936.
[29] Li, Q.; Liu, X.; Zhao, L.; Lei, Z.; Lu, Z.; Guo, L. A novel vibration sensor based on phase grating interferometry. *Appl. Phys. B-Lasers O* **2017**, *123*, 162.
[30] Khan, M. F.; Knowles, B.; Dennison, C. R.; Ghoraishi, M. S.; Thundat, T. Pressure modulated changes in resonance frequency of microchannel string resonators. *Appl. Phys. Lett.* **2014**, *105*, 013507.
[31] Wakiwaka, H.; Takeuchi, T.; Ito, N.; Tashiro, K.; Makimura, M.; Kiyomiya, T. Development of a Frequency Change Output Type Sensor Device by Pressure Change Using SmFe Thin Film. *Sens. Lett.* **2013**, *11*, 157–160.

Manuscript received: December 25, 2019
Manuscript revised: March 4, 2020
Manuscript accepted: March 8, 2020
Accepted manuscript online: March 11, 2020
Version of record online: April 29, 2020

